

# Image Blind Deblurring Using an Adaptive Patch Prior

Yongde Guo and Hongbing Ma\*

**Abstract:** Image blind deblurring uses an estimated blur kernel to obtain an optimal restored original image with sharp features from a degraded image with blur and noise artifacts. This method, however, functions on the premise that the kernel is estimated accurately. In this work, we propose an adaptive patch prior for improving the accuracy of kernel estimation. Our proposed prior is based on local patch statistics and can rebuild low-level features, such as edges, corners, and junctions, to guide edge and texture sharpening for blur estimation. Our prior is a nonparametric model, and its adaptive computation relies on internal patch information. Moreover, heuristic filters and external image knowledge are not used in our prior. Our method for the reconstruction of salient step edges in a blurry patch can reduce noise and over-sharpening artifacts. Experiments on two popular datasets and natural images demonstrate that the kernel estimation performance of our method is superior to that of other state-of-the-art methods.

**Key words:** blind deblurring; adaptive patch prior; kernel estimation; low-level features; internal patch information

## 1 Introduction

Image capturing is susceptible to physical limitations, such as low lighting, camera shaking, and defocusing. Therefore, captured images are often blurry and noisy. Image blind deblurring is a reverse reconstruction process performed to recover original images from a degraded image taken under unknown blur kernel conditions. Image deblurring has a wide range of applications in various fields, including the biomedical, aerospace, and public safety fields, among many other fields. Thus, the blind deblurring algorithm has practical and research importance and has become a crucial topic of image processing research.

The main issue encountered in blind deblurring processes is the solution of an ill-posed problem with an

- Yongde Guo is with the Department of Electronic Engineering, Tsinghua University, Beijing 100084, China. E-mail: gyd14@mails.tsinghua.edu.cn.
- Hongbing Ma is with the Department of Electronic Engineering, Tsinghua University, Beijing 100084, and the College of Information Science and Engineering, Xinjiang University, Urumqi 830046, China. E-mail: hbma@mail.tsinghua.edu.cn.

\*To whom correspondence should be addressed.

Manuscript received: 2018-06-05; revised: 2018-09-04; accepted: 2018-09-07

observed or external image prior to restoration. Under the assumption that the blur is uniform and linear over the whole image, the relational model between the blurry image  $\mathbf{y}$  and the sharp image  $\mathbf{x}$  can be expressed as

$$\mathbf{y} = \mathbf{k} \otimes \mathbf{x} + \mathbf{n} \quad (1)$$

where  $\mathbf{k}$  is the blur kernel,  $\otimes$  denotes the convolution operator, and  $\mathbf{n}$  is additive noise. In practice, blind deblurring is a bilateral ill-posed problem because the sharp image  $\mathbf{x}$  and blur kernel  $\mathbf{k}$  are unknown in blind deconvolution. Thus, our aim is to estimate the nontrivial solution of a sharp image and a blur kernel from the observed blurry image.

Given that blind deblurring is an ill-posed inverse problem, numerous previous works have assumed various prior knowledge of either the sharp image  $\mathbf{x}$  or blur kernel  $\mathbf{k}$  estimation for a single blurry image. Natural image priors, which are assumed or extracted from the diverse structure of the observed image, have received considerable research interest. Several works<sup>[1–4]</sup> have proposed a sparsity prior based on the assumption that the gradients of a sharp image follow a heavy-tailed distribution. Fergus et al.<sup>[1]</sup> fitted a prior based on a Gaussian mixture model and used variational Bayesian inference to compute a prior distribution.

Shan et al.<sup>[2]</sup> adopted a unified probabilistic model for kernel and latent image estimation. Their method can restore strong edges and suppress the ringing effect. Levin et al.<sup>[3,4]</sup> pointed out that the naive Maximum A Posteriori (MAP) method can generate a trivial solution for the estimation of  $\mathbf{x}$  and  $\mathbf{k}$  and thus introduced an expectation maximization scheme with maximum marginal distribution. Sophisticated results have been obtained by using  $L0$  or  $L1$  norm-based regularization as a prior constraint<sup>[5-7]</sup>. Sparse representation has also been used for blur kernel recovery<sup>[8-10]</sup>.

Another group of methods<sup>[11-15]</sup> based on explicitly edge-based priors can be used to select or predict the salient edge of the observed image for kernel evaluation. Joshi et al.<sup>[11]</sup> exploited strong edge prediction and enhancement to improve blur kernel estimation. Cho and Lee<sup>[12]</sup>, Xu and Jia<sup>[13]</sup>, and Cho et al.<sup>[14]</sup> developed effective edge priors with heuristic edge filtering and selecting strategies. Moreover, a two-stage kernel estimation framework has been implemented<sup>[13]</sup> to enable the optimization of kernel solution and the ability to evaluate large kernels. Zhou and Komodakis<sup>[15]</sup> employed a combination of the Markov Random Field (MRF) image and geometric parsing knowledge as a high-level edge prior to kernel estimation. Although the heuristic edge method is valid in image blind recovery under sufficient edge information conditions, it easily causes noise amplification and image over-sharpening.

A patch-based approach has been widely used in image deblurring to obtain the sophisticated structures of priors. Generally, gradient filters consider only neighboring pixels within a radius of 3 pixels. Given that the patch-based method involves a range of pixels, it is conducive for extracting sophisticated image structures or textures. In addition, a patch-based method is helpful for noise suppression and deblurring improvement in blind deconvolution. Sun et al.<sup>[16]</sup> established a pair of patch priors on the basis of synthetic structures and an external image dataset. The experimental results of their algorithm were better than those of previous algorithms. Michaeli and Irani<sup>[17]</sup> proposed a prior with cross-scale recurrence to identify a sharp patch instead of a blurry one in an internal patch. Lai et al.<sup>[18]</sup> employed a color-line model as a patch prior to enhance the salient edges. Ren et al.<sup>[19]</sup> presented an enhanced low-rank prior, which applied the self-similarity of image patches to restore the latent image. Several special priors have been proposed

recently. These priors include exemplar<sup>[16,20,21]</sup>, image intensity statistics<sup>[22,23]</sup>, semantic segmentation<sup>[24]</sup>, and logarithmic prior<sup>[25]</sup>.

In this paper, we present an adaptive patch prior method for blur kernel estimation from a single image. Our proposed approach is inspired by a pixel transform model<sup>[26]</sup> that decomposes pixels from an image patch into basic elements. In addition, our method can reform low-level features to constrain the strong edges of a blurry patch. We use a simple, novel method to rebuild the step edges of a patch through image segmentation. This procedure drastically improves sharp edges and textures for latent image and kernel estimation. Moreover, we utilize the MAP framework and coarse-to-fine scaling strategy in our restoration process to enable our algorithm to accommodate large kernels and alleviate noise levels. Notably, our prior is a nonparametric model that relies only on internal patch information without other external statistical knowledge. Experimental results demonstrate that the performance of our proposed algorithm in two widely used deblurring datasets and some real-world blurry images is comparable with that of state-of-the-art methods.

This paper is structured as follows. In Section 2, we explain foundational work and present the adaptive patch prior model. In Section 3, we provide an overview of blind deblurring algorithms that are based on the MAP framework. We describe the experimental results obtained by other state-of-the-art methods and the limitations of our algorithm in Section 4. We present our conclusion in the final section.

## 2 Adaptive Patch Prior Model

To approach the ill-conditioned problem of blind deconvolution, the proper prior knowledge of the blurry image is necessary for kernel estimation. Currently, the edge feature is widely used as a prior to induce a salient edge of the latent image. Some heuristic approaches<sup>[12-14]</sup> have the ability to provide a strong edge prediction or enhancement for the restored kernel. These approaches make use of the shock or bilateral filter, which forcibly changes edge structure. Unfortunately, these methods are accompanied by some artifacts, including image over-sharpening and noise exposure in the latent image. We proposed a method for improving blind deblurring performance by remedying these problems.

We present a novel edge-based patch prior to

reconstruct effective low-level features, such as edges, corners, and junction structures, in kernel estimation for obtaining high-quality restoration results without heuristic image filters or external image knowledge. Any observed image pixel can be decomposed in accordance with the properties of the pixel transform model into three basic elements: base patch, image contrast, and mean.

Our work is closely related to that of Ref. [16], which created patch priors on the basis of image primitive method. Sun et al.<sup>[16]</sup> generated two types of patch priors, which are learned from an external image dataset and simulated structures within the image edge and corner. Their patch contrast  $\alpha$  refers to the empirical distribution of the local contrast on the BSDS500 dataset. The major difference between our prior and that of Sun et al.<sup>[16]</sup> is that our adaptive prior is extracted from the local image patch by using image segmentation techniques. In addition, our method does not need an external dataset for reference.

In our approach, step edges in the base patch are reconstructed through image segmentation using the two-dimensional (2D)-Otsu method<sup>[27]</sup>. Given that the derived value of the step edge is less than the extreme values of the blurry patch, a weighted term is introduced to handle step edge values that are as large as possible. Our normalized patch prior could be produced via the pixel transform model when the three basic elements are fixed. In contrast to that of Ref. [16], our adaptive patch prior relies only on internal patch information, which is light, flexible, and accurate for local statistics. An example of our processed patch value distribution and regionalization in a blurry patch is shown in Fig. 1.

### 2.1 Pixel transform model

Our work is motivated by the pixel transform model that serves as the basis for our patch reconstruction. The pixel transform model has been broadly applied for brightness and contrast adjustments in image processing. Pixel transforms can decompose any pixel into three basic elements that comprise base pixel and image parameters (brightness and contrast). The model expression is defined as

$$g(\mathbf{u}) = \alpha f(\mathbf{u}) + \beta \quad (2)$$

where  $\mathbf{u}$  is the input patch pixel, and  $\alpha$  is the gain factor, which is the control pixel contrast. The bias factor  $\beta$  determines pixel brightness. In this case, we take the patch standard deviation and average as the  $\alpha$  and  $\beta$  factors, respectively. The functions  $g(\mathbf{u})$  and  $f(\mathbf{u})$

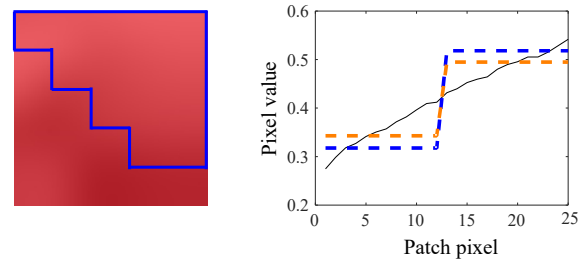


**Fig. 1** Sample of our processed patch value distribution and regionalization in a blurry image patch. The black solid line in the right figure represents the original blurred pixel values. The blue dashed line shows the step edge derived from the internal properties of the blurry patch using our method and is relative to the orange dashed line, which is generated by the ordinary 2D-Otsu method. The blue step edge is close to the extreme values of black line. The blue region represents our segmentation result and is superimposed on the left primitive blurry patch.

are the output and input patches, respectively. Note, however, that  $f(\mathbf{u})$  is the base patch, which removes the average and the standard deviation for the patch pixels. The image decomposition process for the above model is shown in Fig. 2. Our method treats  $g(\mathbf{u})$  as the patch prior. Thus, the key point is determining how to rebuild the base patch  $f(\mathbf{u})$  and the variables  $\alpha$  and  $\beta$  for kernel estimation constraints, as explained in Section 2.2.

### 2.2 Building the base patch

We derive the sharp patch prior  $g(\mathbf{u})$  such that the reconstructed step edge is the core of the base patch  $f(\mathbf{u})$ . Our target is to adaptively build the step edge without external patch statistics, which, as pointed out by Ref. [28], has no more predictive power than internal statistics. We use a simple, novel method to generate the base patch  $f(\mathbf{u})$  via image segmentation from the observed image. Image segmentation is widely applied in computer vision and has also inspired similar research in blind deblurring. Joshi et al.<sup>[29]</sup> and Lai et al.<sup>[18]</sup> employed a  $k$ -means clustering method via a color-line model to perform nonblind and blind image deconvolution.

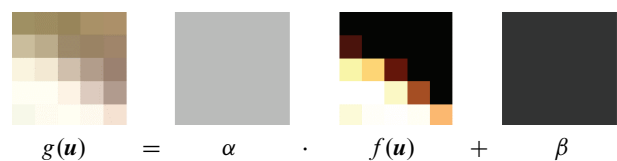


**Fig. 2** Image patch decomposition for the pixel transform model. The processed patch  $g(\mathbf{u})$  is derived from the base patch  $f(\mathbf{u})$  multiplied by the standard deviation  $\alpha$  of the latent image and added to its average  $\beta$ . In blind deconvolution, we regard  $g(\mathbf{u})$  as the image patch prior.

The threshold  $T$  is calculated using the 2D-Otsu method<sup>[27]</sup> to continue building the base patch. Then, each patch pixel  $\mathbf{u}_i$  is divided into two classes by thresholding. The generation of the base patch  $f(\mathbf{u})$  can be written as

$$m_{ij} = \begin{cases} 1, & \text{if } \mathbf{u}_i \geq T; \\ 0, & \text{otherwise;} \end{cases}$$

$$s_0 = \frac{\sum_i m_{i0} \mathbf{u}_i}{\sum_i m_{i0}}, \quad s_1 = \frac{\sum_i m_{i1} \mathbf{u}_i}{\sum_i m_{i1}},$$

$$f(\mathbf{u}) = \frac{m_{ij} \cdot s_j - \mu_s}{\sigma_s} \quad (3)$$

where  $m_{ij}$  denotes the mask divided into  $j$  classes at the number  $i$  of patch pixels,  $s_0$  and  $s_1$  represent the centers of two classes in the vector of the image patch  $\mathbf{u}$ , and the contrast  $\sigma_s$  and brightness  $\mu_s$  are derived from the segmented patch. With this base patch, we adopt the 2D-Otsu method, which is superior to the original Otsu approach and could suppress noise.

### 2.3 Modeling the adaptive patch prior

In principle, the base patch  $f(\mathbf{u})$  is obtained in Eq. (3), and all variables are substituted into Eq. (2) to complete prior generation. Nevertheless, we note that the above procedure leads to inconspicuous results after the implementation of kernel estimation mainly because the range of our preliminary patch is less than that of the blurry image patch. Thus, we introduce an additional weighted term  $\|s_0 - s_1\|_2^2$  for the calculation of the large step edge. This term can increase the prior range to approximate the latent image patch range, as shown in Fig. 1.

Hence, the base patch  $f$ , the weighted term  $\|s_0 - s_1\|_2^2$ , and  $\mu_p$  and  $\sigma_p$ , the average and standard deviation from input patch, respectively, are substituted into Eq. (2). The penalty function of our prior is written as follows:

$$\rho(\mathbf{P}) = \frac{\sum_{i \in \mathbf{P}} \sum_{j=0}^1 \|m_{ij} \mathbf{P}_i - (f(\mathbf{P}_i) \sigma_p + \mu_p)\|_2^2}{\|s_0 - s_1\|_2^2} \quad (4)$$

where  $\mathbf{P}$  is an input patch, and the denominator term  $\|s_0 - s_1\|_2^2$  is the normalized weight of the centers of two classes, whose role is to increase the distance between the two classes. Overall, our priors offer strong blind deblurring performance, as demonstrated in the following experimental section. The blue dashed line shown in Fig. 1 represents the performance of our prior.

### 3 Blind Kernel Estimation

The MAP estimation framework is used for kernel evaluation in our blind deblurring algorithm. We employ an alternate iterative scheme to solve for the sharp image  $\mathbf{x}$  and kernel  $\mathbf{k}$  until they converge. In this scheme, we use a coarse-to-fine scaling strategy, which avoids the problems of a local minimum and large kernel handling. Our patch prior also plays an important role in kernel estimation given that a sharp step edge is reformed by image segmentation and weight normalization. Moreover, edge mask selection, which can exclude the useless edges in recovery, is required before patch prior calculation. After blur kernel estimation is completed, we employ nonblind deconvolution to solve for the sharp image. The whole algorithm framework is shown in Fig. 3.

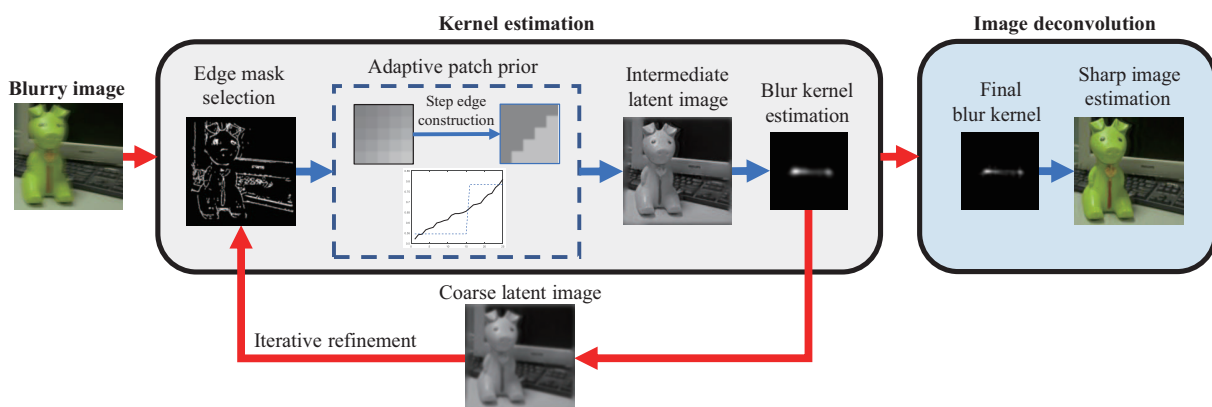


**Fig. 3** Our blind deconvolution framework illustrated in a single image. The MAP scheme and image pyramid scaling strategy are used for blind deblurring. A blurry image is used as input. The refined edge can be extracted on each image scale level through edge selection. The sharp step edge of patch reconstruction is generated using 2D-Otsu. Our adaptive patch prior is generated by the pixel transform model. Then, the latent image and kernel objection function alternately solve for the generated intermediate image and blur kernel until they converge. Finally, the sharp image is restored through nonblind deconvolution with the estimated blur kernel.

### 3.1 Selecting useful edges

Image salient edge information contributes to image deblurring<sup>[2,11–13,16]</sup>. Some edges, however, are not always suitable for kernel estimation<sup>[13]</sup>, or may even hinder accurate kernel evaluation. Therefore, we use the edge-based mask as a useful edge filter in our work. Our edge mask adopts a hybrid approach that is generated by a different edge metric from the latent image gradient, which could be excluded as the most useless edge to accelerate kernel solving. At first, our initial edge mask adopts an  $r$ -map that is computed on each image scale level in accordance with a previously reported method<sup>[13]</sup>. The  $r$ -map can filter out useless edges when flat regions or spikes appear. In the next step, we apply a filter bank<sup>[16]</sup> as a refined mask that uses directional Gaussian derivatives in the latent image gradient. In the final step, our mask combines the former two approaches for latent image estimation and then rules out pixel ambiguity by setting a threshold  $t$  for the gradient magnitude before kernel computation. Refined edge locations are found on the basis of the above edge mask process and are involved in our patch prior calculation.

### 3.2 Optimization for kernel estimation

Our goal is the accurate estimation of the blur kernel for a single blurry image  $\mathbf{y}$ . To avoid trivial solutions for both the sharp image  $\mathbf{x}$  and kernel  $\mathbf{k}$  in MAP method, our adaptive patch and Gaussian prior are used to estimate  $\mathbf{x}$  and  $\mathbf{k}$  for nontrivial solutions. Moreover, we introduce the scalable coarse-to-fine strategy to accommodate large kernels and local minima. To yield favorable results, the gradient filter is employed in the deblurring. The objective function for optimization problem solving can be written as

$$(\hat{\mathbf{x}}, \hat{\mathbf{k}}) = \arg \min_{\mathbf{x}, \mathbf{k}} \{ \|\nabla \mathbf{x} \otimes \mathbf{k} - \nabla \mathbf{y}\|^2 + \lambda_x \|\nabla \mathbf{x}\|_2^2 + \lambda_p \sum_n \rho(\mathcal{Q}_n \mathbf{x}) + \gamma \|\mathbf{k}\|_2^2 \} \quad (5)$$

where  $\nabla = \{\partial_x, \partial_y\}$  is the image gradient operator;  $\lambda_x$ ,  $\lambda_p$ , and  $\gamma$  are penalty factors for  $\mathbf{x}$  and  $\mathbf{k}$ ; and  $\mathcal{Q}_n$  extracts the  $n$ -th patch of the vector  $\mathbf{x}$ , which is derived from the latent image  $\hat{\mathbf{x}}$ . The first term is a data term that can force similarity between the observed image and the latent sharp image convolution with blur kernel. This term is followed by two quadratic terms that are used to maintain large gradients and lead to strong edges for latent image recovery. The last term is a Gaussian prior to allow fast kernel calculation. Note that the

sharp image  $\mathbf{x}$  and blur kernel  $\mathbf{k}$  are unknowns in blind deblurring; the Alternate Minimization (AM) method is used effectively for cost minimization in Eq. (5). The estimation of  $\mathbf{x}$  and  $\mathbf{k}$  uses iterative procedures for the MAP solution, as shown in Algorithm 1. We provide additional detail for updating  $\mathbf{x}$  and  $\mathbf{k}$  in the following sections.

### 3.3 Latent image $\hat{\mathbf{x}}$ update

We solve for an intermediate image  $\mathbf{x}$  on each image scale by using the given or previous solution of  $\mathbf{k}$  from the blurred image  $\mathbf{y}$ . Our adaptive patch prior is beneficial for alleviating the ill-conditioned problem in the MAP scheme in the case of sharp edges and textures in the recovery image patch. Our prior also helps reduce noise and improves over-sharpening improvement in the latent image. The objective function of the latent image  $\hat{\mathbf{x}}$  can be designated as

$$\hat{\mathbf{x}} = \arg \min_{\mathbf{x}} \{ \|\nabla \mathbf{x} \otimes \mathbf{k} - \nabla \mathbf{y}\|^2 + \lambda_x \|\nabla \mathbf{x}\|_2^2 + \lambda_p \sum_n \rho(\mathcal{Q}_n \mathbf{x}) \} \quad (6)$$

The last prior term in Eq. (6) could not be solved directly because it is nonlinear. Therefore, we also use the AM approximation method to alternatively update our patch prior term in Eq. (6). In particular, we require this condition to update the variables of the patch prior  $\rho$  in turn. Then, our patch prior could be obtained by using Eq. (4) when fixing all variables in our patch prior.

#### Step 1: Update patch prior variables

In this step, our adaptive patch prior using Eq. (4) contains a nonlinear term. Thus, the variables  $M_{\text{edge}}$ ,  $f$ , and  $r$  are updated in turn. The updating process is as

---

#### Algorithm 1 Blind kernel estimation

---

##### Input:

- $\mathbf{y}$  : Observed image;
- $\mathbf{k}$  : Initial kernel;
- $m$  : Image pyramid level;
- $n$  : Iteration number on each level.

##### Output:

 Latent image  $\hat{\mathbf{x}}$  and kernel  $\hat{\mathbf{k}}$ 

- 1: **for**  $i = 1 \leq m$  **do**
  - 2:     **for**  $j = 1 \leq n$  **do**
  - 3:         Calculate the mixed mask using the  $r$ -map and filter bank methods;
  - 4:         Update intermediate image  $\hat{\mathbf{x}}$  using our adaptive patch prior in Eq. (6);
  - 5:         Filter the latent image gradient via setting threshold  $t$ ;
  - 6:         Update kernel  $\hat{\mathbf{k}}$  using Gaussian prior in Eq. (11);
  - 7:     **end for**
  - 8:     Upsample kernel  $\hat{\mathbf{k}}^{i+1}$ .
  - 9: **end for**
-

follows:

(1) Generate the edge mask  $M_{\text{edge}}$ : The generation of the mixed mask  $M_{\text{edge}}$  consists of the  $r$ -map<sup>[13]</sup> and filter bank<sup>[16]</sup> methods.  $M_r$  filters out useless edges, and  $M_{\text{filter}}$  removes gradient noise. The edge mask can locate a useful edge position for our patch prior application.

(2) Build the step edge of the base patch  $f$ : For each patch, the 2D-Otsu<sup>[27]</sup> method is employed to segment the patch pixel into two classes, namely,  $s_0$  and  $s_1$ . The segment results, however, are smaller than the extreme values of the blurry patch. Therefore, the weighted term  $\|s_0 - s_1\|_2^2$  is introduced to extend the distance between the two classes  $s_0$  and  $s_1$  in Eq. (4).

(3) Update the vector of reconstructed patch  $r_n$  using the pixel transform model: The contrast  $\sigma_p$  and brightness  $\mu_p$  are obtained from the latent image patch. At the  $n$ -th patch of the image, after fixing the above factors, the reconstructed patch  $r_n$  could be obtained by

$$r_n = f^n \sigma^n + \mu^n \quad (7)$$

### Step 2: Compute latent image $\hat{x}$

While our patch prior parameters are already updated in Eq. (7), the next step is solving for the latent image  $\hat{x}$  with our prior.

$$\rho(Q_n x) = \frac{\|Q_n x - r_n\|_2^2}{\|s_0^n - s_1^n\|_2^2} \quad (8)$$

Setting the derivation of  $\hat{x}$  equal to 0 in Eq. (6) enables the equation to be rewritten in matrix form as

$$\begin{aligned} ((K^T K + \lambda_x)G + \lambda_p \sum_n \frac{Q_n^T Q_n}{\|s_0^n - s_1^n\|_2^2}) \hat{x} = \\ K^T G Y + \lambda_p \sum_n \frac{Q_n^T r_n}{\|s_0^n - s_1^n\|_2^2} \end{aligned} \quad (9)$$

where  $K$  and  $Y$  are the matrix forms of the blur kernel  $k$  and the blurry image, respectively. The gradient operator matrix  $G = G_x^T G_x + G_y^T G_y$ . Given that our prior contains nonlinear terms that cannot be solved in closed form, the biconjugate gradient method is used to solve this equation.

### 3.4 Kernel $\hat{k}$ update

After the latent image  $\hat{x}$  is generated, we update the kernel  $\hat{k}$ . To reduce noise in kernel estimation, we set a threshold  $t$  to rule out a small gradient magnitude of  $\hat{x}$  by using a previously reported method<sup>[13]</sup>. The selecting edge of the latent image gradient  $\nabla x^m$  is defined as

$$\nabla x^m = \nabla \hat{x} \cdot U(M_{\text{edge}} \|\nabla \hat{x}\|_2 - t) \quad (10)$$

where  $U$  is the unit step function, which equals 1 for positive values and equals 0 otherwise.

Gaussian prior is used to find a fast and simple solution for kernel estimation. After disregarding the  $x$  term in Eq. (5), the objective function of kernel  $\hat{k}$  can be represented as

$$\hat{k} = \arg \min_k \{ \|\nabla x^m \otimes k - \nabla y\|_2^2 + \gamma \|k\|_2^2 \} \quad (11)$$

Similarly, other approaches<sup>[10, 12, 16, 17]</sup> have used  $L_2$ -norm regularization, which can be directly and effectively computed in closed-form solution by using fast Fourier transforms.

## 4 Experimental Results

We examine the performance of our algorithm by using the datasets of Levin et al.<sup>[4]</sup> and Sun et al.<sup>[16]</sup> We compare the performance of our algorithm with that of state-of-the-art methods<sup>[1, 3, 5, 10, 12, 13, 16–18, 22, 25]</sup>. We also test the blind deblurring performance of our approach on some natural blurred images under an unknown blur kernel. In addition, we test the kernel estimation performance of the provided code or other testing methods on the above two datasets to enable fair comparison. Our experiment applies a previously described default setting<sup>[3, 16]</sup> and uses the corresponding nonblind deconvolution algorithm<sup>[3, 30]</sup>. We adopt the meaning of error ratio<sup>[4]</sup>, Peak Signal-to-Noise Ratio (PSNR), Structural Similarity (SSIM), and success rate scores as indices of quantitative evaluation. We apply subjective visual judgment as qualitative evaluation.

### 4.1 Image deblurring for a synthetic dataset

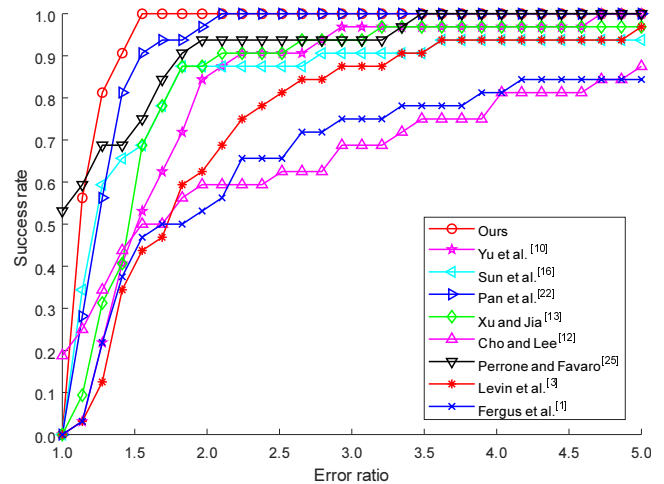
In implementation, our algorithm estimates the blur kernel by using an image pyramid, which can create a multiscale level of images to avoid the local minima. We shrink the blurry image with a down-sampling factor  $r = \frac{1}{\sqrt{2}}$  until the relevant kernel size is  $3 \times 3$  pixels. At each scaling level, the latent image  $\hat{x}$  and kernel  $\hat{k}$  are alternately updated in seven iterations. For  $\hat{x}$  estimation, we use our prior to adaptively obtain the required variables in the patch except for the setting patch size to  $5 \times 5$  pixels. We empirically set the parameters  $\lambda_x$  and  $\lambda_p$  to gradually decrease from 0.2 to 0.1 and 0.01 to 0.001, respectively, in Eq. (9). After solving for  $\hat{x}$ , we compute the gradient direction of  $\hat{x}$  into four groups by using a threshold that holds at least  $2\sqrt{N_k}$  pixels in each gradient angle, where  $N_k$  is the number of kernel elements. For the  $\hat{k}$  computation, we

choose  $\gamma = 1$  in Eq. (11).

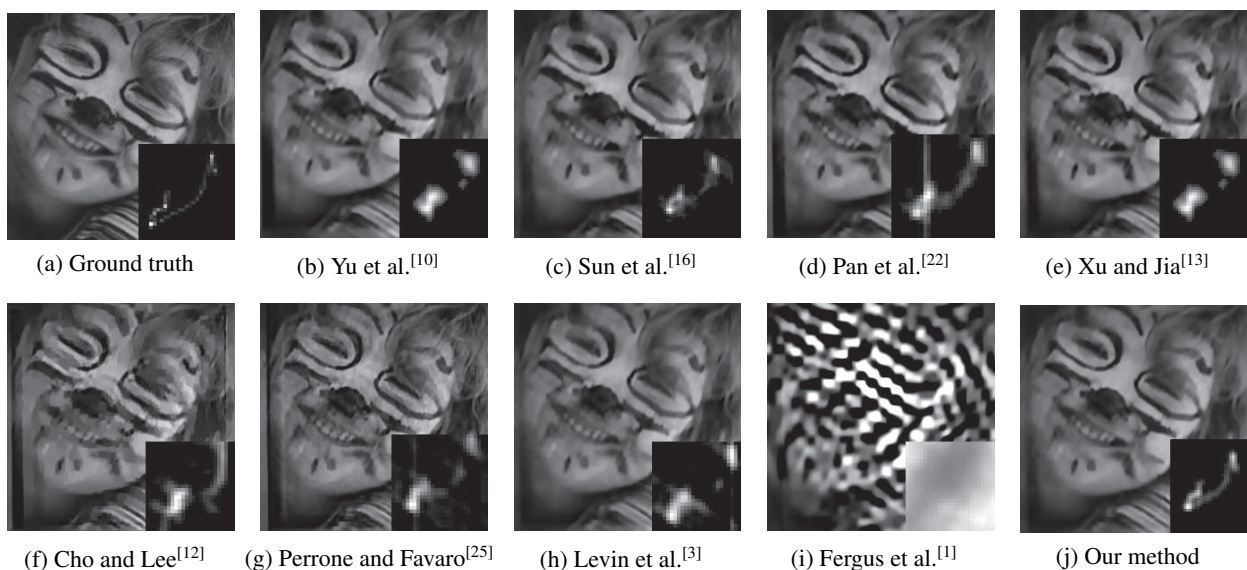
The first set of tests was performed on the Levin et al.<sup>[4]</sup> dataset, which has 32 blurry images. The size of each image was defined in Ref. [4] as  $255 \times 255$  pixels with eight different kernels from  $13 \times 13$  pixels to  $27 \times 27$  pixels. We assume that all the kernels have size of  $51 \times 51$  pixels in this test. We use sparse deconvolution<sup>[3]</sup> for the final sharp image recovery to avoid obtaining biased recovery results with different nonblind deconvolution methods. The deblurring results of our algorithm and those of other algorithms are displayed in Fig. 4. Our method can precisely estimate the blur kernel, which is close to the ground truth. Success rate can be defined as an error ratio of less than  $3^{[4]}$ . As shown in Fig. 5, our approach not only demonstrates the best performance among all other methods but also has a low error ratio and high success rate for blind kernel restoration on the Levin et al.<sup>[4]</sup> dataset. We also provide the quantitative measurements of the tested algorithms in Table 1.

Another set of tests was performed on the Sun et al.<sup>[16]</sup> dataset, which contains 640 large blurry images that are based on the eight kernels of Levin et al.<sup>[4]</sup> with 1% additive Gaussian noise. Given that the dataset consists of different scene images, kernel estimation becomes increasingly diverse and challenging. In this test, we continue to assume that the kernel size is  $51 \times 51$  pixels. We employ the nonblind deconvolution method of Zoran and Weiss<sup>[30]</sup> to restore the final sharp image. Moreover, successful deblurring is set at an error rate under  $5^{[16]}$ . We subject this dataset to

the tested methods, and we plot the cumulative error ratio for quantitative evaluation, as shown in Fig. 6. We also list the quantitative measurement obtained by different methods in Table 2. The comparison of the performances of the tested algorithms on the Sun et al.<sup>[16]</sup> dataset is visually presented in Fig. 7. Our method attains an accurate kernel and high-quality deblurring result and achieves more favorable performance than



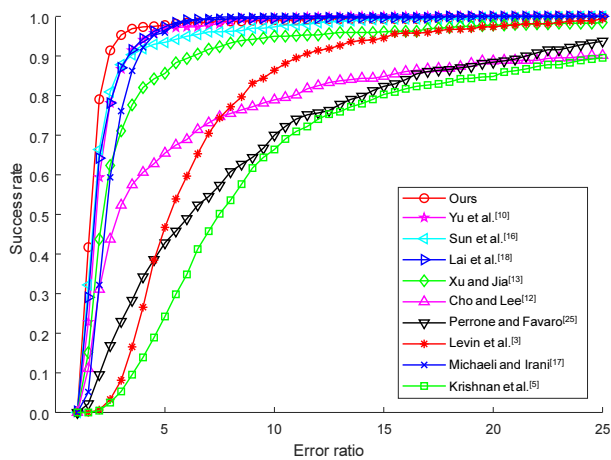
**Fig. 5** Cumulative error ratio distribution for the Levin et al.<sup>[4]</sup> dataset. An approach with an error rate that exceeds 3, has poor performance. Note that the results of Cho and Lee<sup>[12]</sup> and Perrone and Favaro<sup>[25]</sup> have a certain percentage at which the error ratio equals 1, which achieves the performance of ground truth. Overall, however, the performance of our approach is more comprehensive than that of other approaches because its success rate is 100% when the error ratio is under 1.5.



**Fig. 4** Visualization of the deblurring results of other tested methods for the Levin et al.<sup>[4]</sup> dataset. These results show that our kernel outperforms other approaches and eliminates noise interference and ringing artifacts.

**Table 1** Quantitative measurement obtained by various methods for the Levin et al.<sup>[4]</sup> dataset.

Method	Error ratio	Success rate (%)	PSNR (dB)	SSIM
Ours	<b>1.1735</b>	<b>100.00</b>	32.0684	0.9202
Yu et al. <sup>[10]</sup>	1.7166	96.88	30.6060	0.9006
Sun et al. <sup>[16]</sup>	2.2341	90.63	30.8825	0.9030
Pan et al. <sup>[22]</sup>	1.2823	<b>100.00</b>	31.7076	0.9147
Xu and Jia <sup>[13]</sup>	2.1365	93.75	30.7093	0.8974
Cho and Lee <sup>[12]</sup>	2.6688	68.75	29.7056	0.8837
Perrone and Favaro <sup>[25]</sup>	1.2024	93.75	<b>32.4780</b>	<b>0.9375</b>
Levin et al. <sup>[3]</sup>	2.0583	87.35	30.0500	0.8960
Fergus et al. <sup>[1]</sup>	13.5268	75.00	28.3758	0.8451

**Fig. 6** Cumulative error ratios of the compared methods on the Sun et al.<sup>[16]</sup> dataset. The success rate and error ratio of our method are superior to those of other methods.

the compared approaches.

## 4.2 Image deblurring for real-world images

In addition to experimenting on synthetic datasets, we also apply our algorithm on natural blurred images

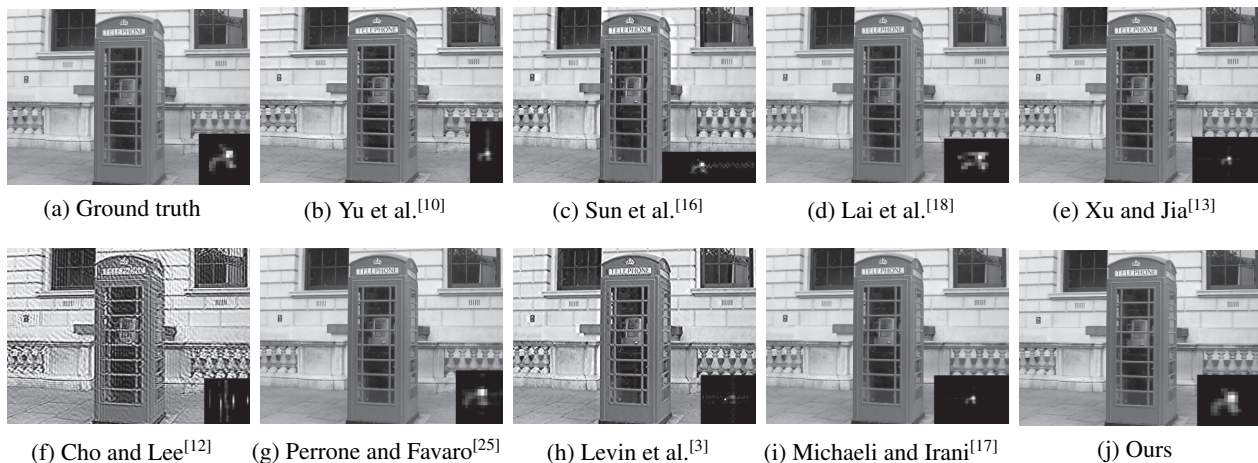
**Table 2** Quantitative comparison of the performance of the tested methods on the Sun et al.<sup>[16]</sup> dataset. Our method outperforms other test approaches.

Method	Error ratio	Success rate (%)	PSNR (dB)	SSIM
Ours	<b>1.8980</b>	<b>97.81</b>	<b>30.1538</b>	<b>0.8610</b>
Yu et al. <sup>[10]</sup>	2.2182	96.88	29.4183	0.8518
Sun et al. <sup>[16]</sup>	2.3764	93.44	29.5279	0.8533
Lai et al. <sup>[18]</sup>	2.1248	97.34	29.6081	0.8421
Xu and Jia <sup>[13]</sup>	3.6293	85.63	28.3135	0.8492
Cho and Lee <sup>[12]</sup>	8.6901	65.47	26.2353	0.8138
Perrone and Favaro <sup>[25]</sup>	9.3687	42.81	24.4213	0.6581
Levin et al. <sup>[3]</sup>	6.5577	46.72	24.9410	0.7952
Michaeli and Irani <sup>[17]</sup>	2.5662	95.94	28.6210	0.8279
Krishnan et al. <sup>[5]</sup>	12.0234	24.22	23.1708	0.7540

under an unknown kernel. In this test setting, we also utilize the nonblind deconvolution of Zoran and Weiss<sup>[30]</sup> to recover a sharp image. The given kernel size varies in accordance with different real-world images. We also apply comparative algorithms, including those provided by Yu et al.<sup>[10]</sup>, Sun et al.<sup>[16]</sup>, Xu and Jia<sup>[13]</sup>, Pan et al.<sup>[22]</sup>, Levin et al.<sup>[3]</sup>, and Michaeli and Irani<sup>[17]</sup>. The visual examples of deblurring results provided by different testing approaches are shown in Figs. 8 and 9. Our method can restore sharp and detailed textures in deblurred images. Moreover, our blur kernels are estimated accurately and clearly.

## 4.3 Method restriction

Our proposed approach works well with synthetic datasets and real-world images. However, we have observed the following shortcomings of our prior:

**Fig. 7** Visual examples of the results obtained with the tested methods for the Sun et al.<sup>[16]</sup> dataset. In contrast to other methods, our method can accurately estimate the blur kernel with noise artifacts and obtain a sharp deblurred image.



**Fig. 8** Visual deblurring results from the state-of-the-art algorithms on a real-world image. Our estimated kernel compares favorably with other testing approaches.



**Fig. 9** Deblurring of each comparison method on another real-world image. Our method can restore more details and reduce noise in a sharp image.

(1) The evaluated kernel is affected by the quantity and quality of image edges. Our patch-based prior relies on an effective edge from edge selection. If a blurred image has low quality or insufficient edges, little edge information is retained after mask filtering. This result can lead to incomplete or incorrect kernel estimation.

(2) The range of our reconstructed step edges ignores approximate distribution values in a blurry patch. Our method simply extracts two centers of classes using image segmentation and reforms sharp step edges via the image primitive model. If the blurry patch has complex textures across a broad range of gray levels, however, our approach misses some details. This behavior might not be conducive for kernel estimation.

(3) The choice of the segmentation algorithm determines the performance of the kernel evaluation. In this work, we adopt the 2D-Otsu method to simplify the calculation of our prior. This method, however, is not the best segmentation method. The introduction of a complex segmentation method is expected to greatly increase algorithmic complexity and computing time in the case of an image with thousands of patches.

## 5 Conclusion

We present an adaptive patch prior for single-image blind deblurring. Our prior is based on the model of image primitives. The crucial step of this method is the introduction of patch segmentation, which can build the sharp step edges of the patch to help guide salient edges and textures for kernel estimation. Moreover, our prior is a nonparametric model that does not require external statistical knowledge and depends only on internal patch information. Experimental results indicate that our proposed approach performs more favorably on two synthetic datasets and on real-world images than state-of-the-art methods. In further works, we plan to improve our method's performance by enhancing its limitations.

## References

- [1] R. Fergus, B. Singh, A. Hertzmann, S. T. Roweis, and W. T. Freeman, Removing camera shake from a single photograph, *ACM Transactions on Graphics*, vol. 25, no. 3, pp. 787–794, 2006.
- [2] Q. Shan, J. Jia, and A. Agarwala, High-quality motion deblurring from a single image, *ACM Transactions on Graphics*, vol. 27, no. 3, pp. 15–19, 2008.
- [3] A. Levin, Y. Weiss, F. Durand, and W. T. Freeman, High-quality motion deblurring from a single image, *IEEE Trans. Pattern Anal. Mach. Intell.*, vol. 32, no. 12, pp. 2354–2367, 2011.
- [4] A. Levin, Y. Weiss, F. Durand, and W. T. Freeman, Efficient marginal likelihood optimization in blind deconvolution, in *Proc. IEEE Conf. Computer Vision and Pattern Recognition*, Colorado Springs, CO, USA, 2011, pp. 2657–2664.
- [5] D. Krishnan, T. Tay, and R. Fergus, Blind deconvolution using a normalized sparsity measure, in *Proc. IEEE Conf. Computer Vision and Pattern Recognition*, Colorado Springs, CO, USA, 2011, pp. 233–240.
- [6] J. Pan and Z. Su, Fast  $\ell^0$ -regularized kernel estimation for robust motion deblurring, *IEEE Signal Processing Letters*, vol. 20, no. 9, pp. 841–844, 2013.
- [7] D. Perrone and P. Favaro, Total variation blind deconvolution: The devil is in the details, in *Proc. IEEE Conf. Computer Vision and Pattern Recognition*, Columbus, OH, USA, 2014, pp. 2909–2916.
- [8] M. M. Bronstein, A. M. Bronstein, M. Zibulevsky, and Y. Y. Zeevi, Blind deconvolution of images using optimal sparse representations, *IEEE Trans. Image Processing*, vol. 14, no. 6, pp. 726–736, 2005.
- [9] H. Zhang, J. Yang, and Y. Zhang, Sparse representation based blind image deblurring, in *Proc. IEEE Conf. Multimedia and Expo*, Barcelona, Spain, 2011, pp. 1–6.
- [10] J. Yu, Z. Chang, C. Xiao, and W. Sun, Blind image deblurring based on sparse representation and structural self-similarity, in *Proc. IEEE Conf. Acoustics, Speech and Signal Processing*, New Orleans, LA, USA, 2017, pp. 1328–1332.
- [11] N. Joshi, R. Szeliski, and D. J. Kriegman, PSF estimation using sharp edge prediction, in *Proc. IEEE Conf. Computer Vision and Pattern Recognition*, Anchorage, AK, USA, 2008, pp. 1–8.
- [12] S. Cho and S. Lee, Fast motion deblurring, *ACM Transactions on Graphics*, vol. 28, no. 5, pp. 89–97, 2009.
- [13] L. Xu and J. Jia, Two-phase kernel estimation for robust motion deblurring, in *Proc. European Conf. Computer Vision*, 2010, pp. 157–170.
- [14] T. S. Cho, S. Paris, B. K. Horn, and W. T. Freeman, Blur kernel estimation using the radon transform, in *Proc. IEEE Conf. Computer Vision and Pattern Recognition*, Colorado Springs, CO, USA, 2011, pp. 241–248.
- [15] Y. Zhou and N. Komodakis, A MAP-estimation framework for blind deblurring using high-level edge priors, in *Proc. European Conf. Computer Vision*, Cham, Switzerland, 2014, pp. 142–157.
- [16] L. Sun, S. Cho, and J. Wang, Edge-based blur kernel estimation using patch priors, in *Proc. IEEE Conf. Computational Photography*, Cambridge, MA, USA, 2013, pp. 1–8.
- [17] T. Michaeli and M. Irani, Blind deblurring using internal patch recurrence, in *Proc. European Conf. Computer Vision*, Cham, Switzerland, 2014, pp. 783–798.
- [18] W. S. Lai, J. J. Ding, Y. Y. Lin, and Y. Y. Chuang, Blur kernel estimation using normalized color-line prior, in *Proc. IEEE Conf. Computer Vision and Pattern Recognition*, Boston, MA, USA, 2015, pp. 64–72.
- [19] W. Ren, X. Cao, J. Pan, X. Guo, W. Zuo, and M. Yang,

- Image deblurring via enhanced low-rank prior, *IEEE Trans. Image Processing*, vol. 25, no. 7, pp. 3426–3437, 2016.
- [20] Y. Hacoen, E. Shechtman, and D. Lischinski, Deblurring by example using dense correspondence, in *Proc. IEEE Conf. Computer Vision*, Sydney, Australia, 2013, pp. 2384–2391.
- [21] T. Kenig, Z. Kam, and A. Feuer, Blind image deconvolution using machine learning for three-dimensional microscopy, *IEEE Trans. Pattern Anal. Mach. Intell.*, vol. 32, no. 12, pp. 2191–2204, 2010.
- [22] J. Pan, D. Sun, H. Pfister, and M. H. Yang, Blind image deblurring using dark channel prior, in *Proc. IEEE Conf. Computer Vision and Pattern Recognition*, Las Vegas, NV, USA, 2016, pp. 1628–1636.
- [23] Y. Yan, W. Ren, Y. Guo, R. Wang, and X. Cao, Image deblurring via extreme channels prior, in *Proc. IEEE Conf. Computer Vision and Pattern Recognition*, Honolulu, HI, USA, 2017, pp. 6978–6986.
- [24] W. Ren, J. Pan, X. Cao, and M. Yang, Video deblurring via semantic segmentation and pixel-wise non-linear kernel, in *Proc. IEEE Conf. Computer Vision*, Venice, Italy, 2017, pp. 1086–1094.
- [25] D. Perrone and P. Favaro, A logarithmic image prior for blind deconvolution, *International Journal of Computer Vision*, vol. 117, no. 2, pp. 159–172, 2016.
- [26] R. Szeliski, *Computer Vision: Algorithms and Applications*. Springer Science+Business Media, 2010.
- [27] J. Liu, W. Li, and Y. Tian, Automatic thresholding of gray-level pictures using two-dimension Otsu method, in *Proc. IEEE Conf. Circuits and Systems*, Shenzhen, China, 1991, pp. 325–327.
- [28] M. Zontak and M. Irani, Internal statistics of a single natural image, in *Proc. IEEE Conf. Computer Vision and Pattern Recognition*, Colorado Springs, CO, USA, 2011, pp. 977–984.
- [29] N. Joshi, C. L. Zitnick, R. Szeliski, and D. J. Kriegman, Image deblurring and denoising using color priors, in *Proc. IEEE Conf. Computer Vision and Pattern Recognition*, Miami, FL, USA, 2009, pp. 1550–1557.
- [30] D. Zoran and Y. Weiss, From learning models of natural image patches to whole image restoration, in *Proc. IEEE Conf. Computer Vision and Pattern Recognition*, Barcelona, Spain, 2011, pp. 479–486.



**Yongde Guo** received the BEng degree from Northeastern University, Shenyang, China, in 2011, and MSc degree in information and communication engineering from Tsinghua University, Beijing, China, in 2014. He is currently working toward the PhD degree in the Department of Electronic Engineering,

Tsinghua University, Beijing, China. His research interests cover image processing, pattern recognition, and spatial information processing.



**Hongbing Ma** received the PhD degree from Peking University, China, in 1999. He is currently an associate professor with the Department of Electronic Engineering, Tsinghua University, China. His main research interest covers image processing, pattern recognition, and spatial information processing and application.